

A Steerable Filter Bank Approach to Endmembers Estimation in Imaging Spectroscopy

Ivica Kopriva¹ and Danielle Nuzillard²

¹Division of Laser and Atomic R&D, Ruđer Bošković Institute, Zagreb, Croatia

²CReSTIC, UFR Sciences Exactes et Naturelles, Moulin de la Housse, BP 1039, 51687, Reims, CEDEX 2, France

ABSTRACT

Estimation of pure spectral signatures, called endmembers, is a key step in hyperspectral image (HI) analysis. We propose endmembers estimation method that uses Gabor Filter Banks (GFBs) to filter HI into set of HIs with different resolutions and orientations. Afterwards, set of approximate pure pixels is identified from each filtered HI by means of directivity based criterion. Hierarchical clustering is used to estimate candidate endmembers from sets of approximate pure pixels. Final estimate of endmembers is obtained after annotation of candidate endmembers with library of pure spectral signatures. Thereby, candidate with the smallest angular deviation with respect to corresponding pure spectra is selected as endmember estimate. Proposed method is compared favorably with five endmembers estimation methods using well-understood experimental AVIRIS Cuprite Nevada dataset.

Index Terms— Hyperspectral imaging, Gabor filters, endmembers, spectral unmixing.

1. INTRODUCTION

Hyperspectral sensors produce images up to several hundreds of narrow adjacent spectral bands. They were used for military needs for many years. With the appearance of commercial airborne hyperspectral imaging systems new applications in resource management, agriculture, mineral exploration and environmental monitoring have emerged [1]. Thereby, algorithms that separate pixel from hyperspectral image into collection of pure spectral signatures, called endmembers, and fractional abundances are of central interest [2], [3]. Provided that scattering among distinct endmembers is negligible and the surface is partitioned according to fractional abundances the spectrum of each pixel $\mathbf{x}_p \in \mathbb{R}_{0+}^{L \times 1}$, $p=1, \dots, P$, is well approximated by linear mixture of endmember spectra weighted by corresponding abundances [2], [3], [4]:

$$\mathbf{x}_p = \sum_{j=1}^J \mathbf{m}_j s_{jp} \quad (1)$$

where $\mathbf{m}_j \in \mathbb{R}_{0+}^{L \times 1}$ stands for pure spectra of the j th endmember, J stands for overall number of endmembers, L stands for number of spectral bands and abundance s_{jp} stands for percentage of endmember j that is present in the pixel p . Due to the nature of the problem nonnegativity and sum-to-one constraints are imposed on abundances:

$$\mathbf{s}_p \in S = \left\{ \mathbf{s} \in \mathbb{R}^J \mid \mathbf{s} \geq \mathbf{0}, \mathbf{s}^T \mathbf{1} = 1 \right\} \quad (2)$$

where S denotes the feasible set of abundance vectors [3]. Annotation of spectra of extracted endmembers with appropriate spectral library enables identification of the components present in a scene covered by acquired image. Provided that endmembers spectra are estimated accurately abundances can be obtained by solving constrained least square problem [3], [4], [5]:

$$\hat{\mathbf{s}}_p = \arg \min_{\mathbf{s}_p \in S} \left\| \mathbf{x}_p - \mathbf{M} \mathbf{s}_p \right\|_2^2 \quad (3)$$

where $\mathbf{M} \in \mathbb{R}_{0+}^{L \times J}$ stands for matrix of endmembers spectra. Thus, knowledge of \mathbf{M} is of key importance for hyperspectral image analysis. To this end, many state-of-the-art algorithms for estimation of endmembers spectra rely on pure pixel assumption [6], [7], [8]. This assumption implies that each endmember is present in at least one pixel alone. Thus, algorithms such as N-FINDR [6], vertex component analysis (VCA) [7], successive volume maximization (SVMAX) [8] and simultaneous orthogonal matching pursuit (SOMP) [9] employ various pure pixels search strategies in estimation of the endmembers. However, pure pixel assumption does not often hold, e.g., in a scene consisting of highly mixed minerals and that occurs due to limited spatial resolution of hyperspectral cameras [3]. We propose method for endmembers estimation that: (i) is using Gabor filter banks (GFBs) parameterized with

different resolutions and spatial orientations to perform spectral band-wise filtering of original hyperspectral image; (ii) owing to complex nature of Gabor filters is using geometric concept of direction to locate, within pre-specified tolerance, approximate pure pixels in each filtered hyperspectral image; (iii) is using hierarchical clustering to group approximate pure pixels and that yields endmembers candidates; (iv) annotates endmember candidates with a library of pure spectra and selects as endmember estimate the candidate with the smallest spectrum angular deviation (SAD) with respect to corresponding pure spectra in the library.

2. METHODOLOGY

2-D Gabor filters are used due to their ability to realize multichannel filtering and decomposing an input spectral images into sparse images containing intensity variation over narrow range of frequency and orientation [10]. The Gabor filters have the following real and imaginary parts respectively:

$$\begin{aligned} R(u, v) &= G(u, v) \cdot \cos((\pi/\sigma)\phi(u, v)) \\ I(u, v) &= G(u, v) \cdot \sin((\pi/\sigma)\phi(u, v)) \quad u, v = -N, \dots, N \end{aligned} \quad (4)$$

where $G(u, v) = \exp(-(u^2 + v^2)/2\sigma^2)$. N stands for size of the filter kernel. The parameter q regulates one of the Q spatial orientations. The parameter $\sigma = \sqrt{2}^{\omega}$, with $\omega=1, 2, \dots, \Omega$, regulates one of the Ω spatial frequencies. Thus, GFB is characterized with a triplet (N, Ω, Q) and is comprised of $Z=\Omega \times Q$ complex filters. When hyperspectral image $\mathbf{X} \in \mathbb{R}_{0+}^{P_1 \times P_2 \times L}$ is processed by GFB each spectral image with the size of $P=P_1 \times P_2$ pixels is filtered separately. That yields complex image which can be written in vectorized form as $\mathbf{Y}_z \in \mathbb{C}^{L \times P_1 P_2}$:

$$\mathbf{Y}_z = \mathbf{M}R_z(u, v) * \mathbf{S} + \sqrt{-1} \times \mathbf{M}I_z(u, v) * \mathbf{S} \quad z=1, \dots, Z \quad (5)$$

where R_z and I_z stand for real and imaginary part of the z^{th}

complex Gabor filter as in (4), $\mathbf{S} \in \mathbb{R}_{0+}^{J \times P_1 P_2}$ is matrix of abundances and "*" stands for 2D convolution operator. Since filtered spectral images are sparse their pixels are natural candidates for approximate pure pixels. Owing to complex nature of Gabor filters we use geometric concept of direction to

locate approximate pure pixel candidates in $\{\mathbf{Y}_z\}_{z=1}^Z$. The criterion is based on the notion that the real and imaginary parts of the complex vector of mixtures point either in the same or opposite directions at the locations of pure pixels [11]. Thus, approximate

pure pixel candidates are located by measuring angular deviation of real and imaginary parts of pixels $\{\mathbf{y}_{pz}\}_{p=1}^P$ from directions of 0 or 180 degrees within the pre-specified tolerance $d\theta$:

$$\left| \frac{R(\mathbf{y}_{pz})^T I(\mathbf{y}_{pz})}{\|R(\mathbf{y}_{pz})\| \|I(\mathbf{y}_{pz})\|} \right| \geq \cos(d\theta) \quad (6)$$

With the value of $d\theta$ we can control degree of purity of pure pixel candidates. If $d\theta$ is too small it can occur that no pure pixel candidates are found. Thus, in addition to triplet (N, Ω, Q) approximation parameter $d\theta$ is also used in parameterization of the estimation of the endmembers candidates. We denote by S_z set of approximate pure pixels located in filtered image \mathbf{Y}_z by using criterion (6). At these locations real parts of \mathbf{Y}_z approximately correspond with endmembers spectra, i.e. $R(\mathbf{y}_{pz})_{p \in S_z} \approx \mathbf{m}_{jS_{jp}}, j \in \{1, \dots, J\}$. Thus, we use hierarchical clustering, implemented in Matlab command `clusterdata`, to group real parts of approximate pure pixels in S_z into predefined number of J cluster centers. That yields estimate of the endmembers candidates $\hat{\mathbf{M}}_z$ found in filtered image \mathbf{Y}_z . Afterwards, we use the U.S. Geological Survey (USGS) Library, [12] to annotate endmembers candidates. Let us denote the spectral library composed of K spectra as: $\mathbf{V} := \{\mathbf{v}_k \in \mathbb{R}_{0+}^{L \times 1}\}_{k=1}^K$. We annotate each endmember candidate $\{\hat{\mathbf{m}}_{jz}\}_{j=1}^J$ with the spectral library: $\hat{\mathbf{m}}_{jz} \leftrightarrow \mathbf{v}_{k_{jz}^*}$ such that:

$$k_{jz}^* = \arg \min_{k=1, \dots, K} \alpha_{jk} = \cos^{-1} \left(\left(\mathbf{v}_k^T \hat{\mathbf{m}}_{jz} \right) / \left(\|\mathbf{v}_k\| \|\hat{\mathbf{m}}_{jz}\| \right) \right) \quad (7)$$

where α_{jk} is SAD, i.e. angle between $\hat{\mathbf{m}}_{jz}$ and \mathbf{v}_k . Thus, after annotation we obtain ordered triples: $\left\{ \left(\hat{\mathbf{m}}_{jz}, k_{jz}^*, \alpha_{jk_{jz}^*} \right) \right\}_{j=1}^J$.

Final endmembers estimates are obtained according to: $\{\hat{\mathbf{m}}_{jz} \leftrightarrow \mathbf{v}_n\}_{j,z=1}^{J,Z}$, such that:

$$n = \arg \min_{k_{jz}^*} \alpha_{jk_{jz}^*} \quad (8).$$

3. EXPERIMENTAL RESULTS

We compare GFBs-based method with N-FINDR, VCA, SVMAX, and SOMP algorithms on the AVIRIS Cuprite Nevada dataset [13]. The VCA algorithm has been used with SNR=10 dB, but other values (20 dB) yielded similar results. In particular we have used the Rcuprite subset

accompanied with [2] and available at http://www.lx.it.pt/~bioucas/code/unmixing_overview.zip. The image is of the size of 250 lines by 191 columns by 188 spectral bands (noisy bands were removed). The Cuprite site is well understood mineralogically [14], [15]. We have been focused on estimating endmembers spectra related to the minerals: Alunite GDS84, Alunite GDS82, Buddingtonite GDS85, Chalcite WS272, Kaolinite KGa1, Muscovite GDS107, Chalcedony CU91 6A and Hematite GDS76. The value for number of endmembers present in the scene J , it is also known as virtual dimension [16], depends on the method used for its estimate as well as on predefined value of the probability of false alarm. It is shown in [15], Table VIII, that for Cuprite dataset applies $8 \leq J \leq 22$. In order not to lose some endmember, we set $J=22$. We have used GFBs with the following parameters: $N \in \{5, 7, 9, 11\}$, $\Omega \in \{2, 4\}$ and $Q \in \{4, 8\}$. Thus, in overall, there were 16 GFBs. We have been selecting pure pixel candidates tolerance $d_0 \in \{3^0, 4^0, 5^0, 6^0, 7^0\}$. We present results, in term of SADs, in Table 1.

TABLE I
ENDMEMBERS ESTIMATION RESULTS FOR AVIRIS CUPRITE DATASET.
REPORTED ARE SADs IN DEGREES. BEST VALUE IS IN BOLD. SECOND BEST VALUE IS UNDERLINED. 'X' MEANS THAT ENDMEMBER IS NOT IDENTIFIED BY PARTICULAR ALGORITHM. *MEAN VALUES ARE ESTIMATED ON FIVE MINERALS THAT WERE IDENTIFIED BY ALL ALGORITHMS.

	GFBs	N- FINDR	VCA	SOMP	SVMAX
Alunite GDS84	2.35	x	x	x	x
Alunite GDS82	3.12	4.38	<u>4.21</u>	4.23	<u>4.21</u>
Buddingtonite GDS85	5.6	4.41	6.24	3.93	<u>3.97</u>
Chalcite WS272	4.42	x	x	x	x
Kaolinite KGa1	7.24	x	x	x	x
Muscovite GDS107	4.52	<u>6.09</u>	6.24	6.56	6.16
Chalcedony CU91 6A	1.89	3.89	<u>2.57</u>	4.05	4.08
Hematite GDS76	2.95	4.01	3.64	3.73	<u>3.33</u>
Mean*	3.61	4.56	4.58	4.50	<u>4.35</u>

True color (RGB) image of the Cuprite site for spectral bands (40, 20, 10) is shown in Figure 1. Proposed GFBs approach to endmembers estimation is overwhelmingly better than other methods. GFBs-based method was the only one able to identify minerals Alunite GDS84, Chalcite WS272 and Kaolinite KGa1. Figure 2 shows pure and some estimated endmembers spectra related to chalcedony CU91 6A mineral. Figure 3 shows pure spectra for Alunite

GDS82, Buddingtonite GDS85 and Chalcedony CU91 6A as well as corresponding endmembers spectra estimated by proposed GFBs method. Figure 4 shows abundances estimated by fully constrained least squares (FCLS) algorithm [17] for five endmembers estimated by proposed GFBs algorithm and SVMAX algorithm. These results provide visual interpretation of SADs reported in Table 1. While less accurate estimate is obtained for Buddingtonite GDS85 for GFBs approach, the SVMAX approach yielded less accurate estimates for other minerals.



Fig. 1. True color image of the Cuprite site for spectral bands (40,20,10).

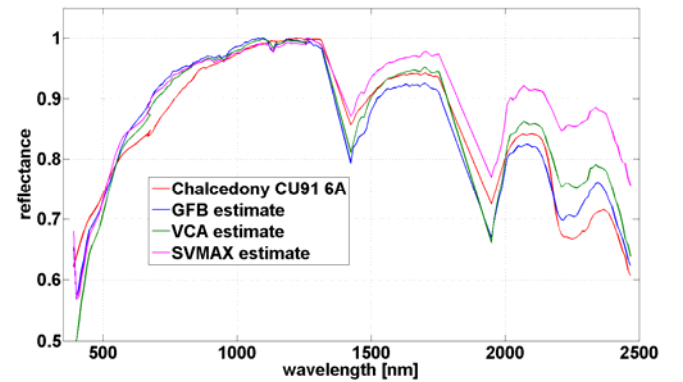


Fig. 2. Pure spectra of chalcedony CU91 6A mineral and endmembers spectra estimated by proposed GFBs method, VCA method and SVMAX method.

4. CONCLUSIONS

The GFBs-based approach to endmembers estimation is proposed. It assumes availability of spectral library but does not impose any assumption on the existence of pure spectra. Instead, multiple GFBs, parameterized in terms of resolution and orientation, can be used to decompose hyperspectral image into sparse images containing intensity variation over narrow range and frequency orientation. In

addition to yield good accuracy in estimation of endmembers GFBs-based approach is suitable for massively parallel implementation. That is, steps (5) to (8) can be implemented concurrently. That makes proposed method suitable for implementation on FPGA-like systems for on board (real time) hyperspectral image analysis.

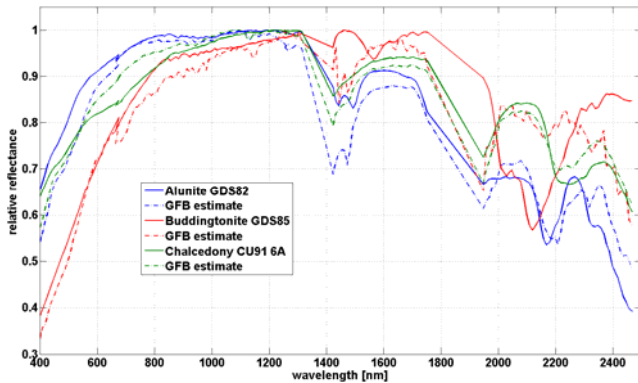


Fig. 3. Pure spectra for Alunite GDS82, Buddingtonite GDS85 and Chalcedony CU91 6A (solid line) as well as corresponding endmembers spectra estimated by proposed GFBs method (dashed line).

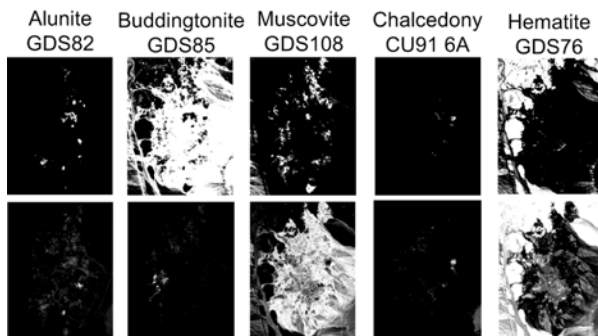


Fig. 4. Abundances estimated by FCLS algorithm for five endmembers estimated by GFBs method (first row) and SVMAX method (second row).

5. ACKNOWLEDGMENTS

This work was supported in part through the FP7-REGPOT-2012-2013-1, Grant Agreement Number 316289 – InnoMol and in part through the Grant 9.01/232 funded by Croatian Science Foundation.

6. REFERENCES

- [1] W.-K. Ma, J.M. Bioucas-Dias, J. Chanussot and P. Gader, "Signal and image processing in hyperpectral remote sensing," *IEEE Sig. Proc. Mag.*, vol. 31, no.1, pp. 22-23, Jan. 2014.
- [2] J.M. Bioucas-Dias, A. Plaza, N. Dobigeon, M. Parente, Q. Du, P. Gader, and J. Chanussot, "Hyperspectral Unmixing Overview: Geometrical, Statistical, and Sparse Regression-Based Approaches," *IEEE J. Sel. Top. Appl. Earth Obs. Remote Sens.*, vol. 5, pp. 354-379, 2012.
- [3] W.-K. Ma, J.M. Bioucas-Dias, T.-H. Chan, N. Gillis, P. Gader, A.J. Plaza, A. Ambikapathi, and C.-Y. Chi, "A Signal Processing Perspective on Hyperspectral Unmixing," *IEEE Sig. Proc. Mag.*, vol. 31, pp. 67-81, 2014.
- [4] N. Keshava, and J.F. Mustard, "Spectral unmixing," *IEEE Sig. Proc. Mag.*, vol. 19, pp. 44-57, 2002.
- [5] D. Heinz, and C.-I. Chang, "Fully constrained least squares linear spectral mixture analysis method for material quantification in hyperspectral imagery," *IEEE Trans. Geosci. Remote Sens.*, vol. 39, pp. 529-545, 2001.
- [6] M. E. Winter, "N-FINDR: An algorithm for fast autonomous spectral endmember determination in hyperspectral data," in *SPIE Conf. Imag. Spectrometry V*, Jul. 1999, vol. 3753, pp. 266-277.
- [7] J. M. P. Nascimento and J. M. Bioucas-Dias, "Vertex component analysis: A fast algorithm to unmix hyperspectral data," *IEEE Trans. Geosci. Remote Sens.*, vol. 43, pp. 898-910, 2005.
- [8] T.-H. Chan, W.-K. Ma, A. Ambikapathi and C.-Y. Chi, "A simplex volume maximization framework for hyperspectral endmember extraction," *IEEE Trans. Geosci. Remote Sens.*, vol. 49, pp. 4177-4193, 2011.
- [9] X. Fu, W. -K. Ma, T. -H. Chan, J. M. Biouca-Dias and M. -D. Iordache, "Greedy Algorithms for Pure Pixels Identification in Hyperspectral Unmixing: A Multiple-Measurement Vector Viewpoint," in *Europ. Sig. Proc. Cong. (EUSIPCO 2013)*, Marrakech, Morocco, September 9-13, 2013, Article no. 14283562, pp. 1-5.
- [10] J. G. Daugman, "Complete Discrete 2-D Gabor Transforms by Neural Networks for Image Analysis and Compression," *IEEE Tr. on Acoust., Speech and Sig. Proc.*, New York, NY, 1988, pp. 1169-1179.
- [11] V. G. Reju, S. N. Koh and I. Y. Soon, "An algorithm for mixing matrix estimation in instantaneous blind source separation," *Sig. Proc.*, vol. 89, pp. 1762-1773, 2009.
- [12] R. Clark, G. Swayze, R. Wise, E. Livo, T. Hoefen, R. Kokaly, and S. Sutley (2007). USGS digital spectral library splib06a: U.S. Geological Survey, Digital Data Series 231. [Online]. Available: <http://speclab.cr.usgs.gov/spectral.lib06>.
- [13] AVIRIS Cuprite Nevada Data set. [Online]. Available: <http://aviris.jpl.nasa.gov/html/aviris/freedata.html>
- [14] G. Swayze, R.N. Clark, F. Kruse, S. Sutley, and A. Gallagher, "Ground-truthing AVIRIS mineral mapping at Cuprite, Nevada," in *Proc. JPL Airborne Earth Science Workshop*, 1992, pp. 47-49.
- [15] G. Martin and A. Plaza, "Spatial-Spectral Preprocessing Prior to Endmember Identification and Unmixing of Remotely Sensed Hyperspectral Data," *IEEE J. Sel. Top. Appl. Earth Obs. Remote Sens.* vol. 5, pp. 380-395, 2012.
- [16] C.-I. Chang and Q. Du, "Estimation of number of spectrally distinct signal sources in hyperspectral imagery," *IEEE Trans. Geosci. Remote Sens.*, vol. 42, pp. 608-619, 2004.
- [17] H. Pu, W. Xa, B. Wang and G.-M. Jiang, "A Fully Constrained Linear Spectral Unmixing Algorithm Based on Distance Geometry," *IEEE Trans. Geosci. Remote Sens.*, vol. 52, pp. 1157-1176, 2014.